Excitation Energy Transfer within Covalent Tetrahedral Perylenediimide Tetramers and Their Intermolecular Aggregates

ARTICLE *in* THE JOURNAL OF PHYSICAL CHEMISTRY C · JULY 2014

Impact Factor: 4.77 · DOI: 10.1021/jp500475c

THE JOURNAL OF PHYSICAL CHEMISTRY C

Article

pubs.acs.org/JPCC

Excitation Energy Transfer within Covalent Tetrahedral Perylenediimide Tetramers and Their Intermolecular Aggregates

Charusheela Ramanan, Chul Hoon Kim, Tobin J. Marks,* and Michael R. Wasielewski*

Department of Chemistry and Argonne-Northwestern Solar Energy Research (ANSER) Center, Northwestern University, Evanston, Illinois 60208-3113, United States

Supporting Information

ABSTRACT: Perylenediimides (PDIs) offer a number of attractive characteristics as alternatives to fullerenes in organic photovoltaics (OPVs), including favorable orbital energetics, high extinction coefficients in the visible spectral region, photostability, and the capacity to self-assemble into ordered nanostructures. However, energy transfer followed by charge separation in PDI assemblies must kinetically out-compete excimer formation that limits OPV performance. We report on the excitation energy transfer (EET) rate in a covalently linked PDI tetramer in which the PDI chromophores are arranged in a tetrahedral geometry about a tetraphenyladamantane core. Transient absorption spectroscopy of the tetramer in CH_2Cl_2 reveals a laser intensity-dependent fast absorption decay component indicative of singlet−singlet annihilation resulting from intramolecular EET. Femtosecond fluorescence anisotropy measurements show that the EET time constant τ = 6 ps, which is similar to that predicted for a through-space Förster EET mechanism. Concentration-dependent steady-state spectroscopic studies reveal the formation of intermolecular aggregates of the tetramers in toluene. The aggregates are formed by cofacial π-stacking interactions between PDIs of neighboring tetramers. Transient absorption spectra of the aggregated tetramers in toluene solution demonstrate long-lived excited-state decay dynamics ($\tau \sim 30$ ns) in agreement with previous observations of PDI excimers.

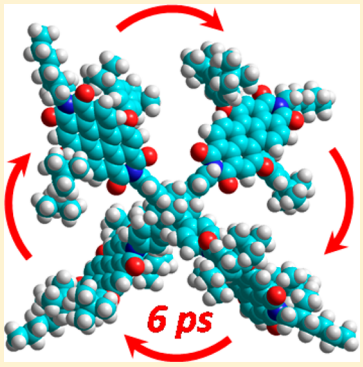

INTRODUCTION

Excitation energy transfer (EET) between chlorophylls in photosynthetic light-harvesting antenna proteins transports excitons to the reaction center protein where they are used to initiate the electron-transfer reactions that provide the chemical potential needed to drive the biochemistry of the organism.[1] Artificial light-harvesting systems are useful models for understanding the structure−function relationships that dictate energy capture and transfer in natural systems.[2,3] The mechanism of EET in both natural and artificial systems is dictated by a variety of factors, including the energy levels of the participating chromophores and their relative distances and orientations.[1,2] Previous work, including our own, has explored these processes in artificial light-harvesting systems employing various chromophores including chlorophylls,[4−6] porphyrins,[7−10] phthalocyanines,[11−13] and rylene dyes.[14,15] These studies have used a variety of molecular scaffolds and bonding motifs, such as covalent bonding,[16−19] hydrogen bonding,[20−22] $\pi-\pi$ stacking,[18,23,24] and dendrimer formation[25−31] to study the role of interchromophore distance and orientation on energy-transfer pathways.

Synthetic light-harvesting systems are also important for developing an understanding of exciton motion with the photoactive layer of organic photovoltaics (OPVs). Recent studies have focused on the design and development of novel synthetic materials for the OPV photoactive layer,[32−37] which consists of domains of electron donor (D) and electron acceptor (A) molecules.[38−40] Within each separate D and A domain, light-absorption creates excitons, which must migrate rapidly and efficiently to the D−A interface, where charge separation occurs.[38−41] As in the natural systems, the optimization of these processes involves manipulation of both energetics and interchromophore geometries.[42−44] Regarding the latter, of particular interest has been the unparalleled success of devices incorporating fullerenes as electron acceptors, specifically in solution-processed devices.[45,46] In addition to being a facile electron-acceptor and having high reported n-type mobilities, they are highly symmetric molecules. Their nearly spherical shape allows for isotropic electron transfer, which can result in a higher statistical chance for beneficial geometrical alignment with the donor molecule.[46] A further argument considers the role of entropic forces in interfacial charge separation, in that the number of electronic states available to a photogenerated electron may be greater than one.[45] Gregg recently extended this idea and modeled the dependence of the equilibrium charge separation free energy with the dimensionality of the organic semiconductor.[47] The results show that equilibrium charge separation becomes more efficient in higher-dimensional materials because of entropy effectively counterbalancing the Coulombic attraction barrier between the photogenerated electron−hole pair. This provides a framework

Special Issue: Michael Grätzel Festschrift

Received: January 15, 2014
Revised: March 3, 2014

   dx.doi.org/10.1021/jp500475c | J. Phys. Chem. C XXXX, XXX, XXX−XXX

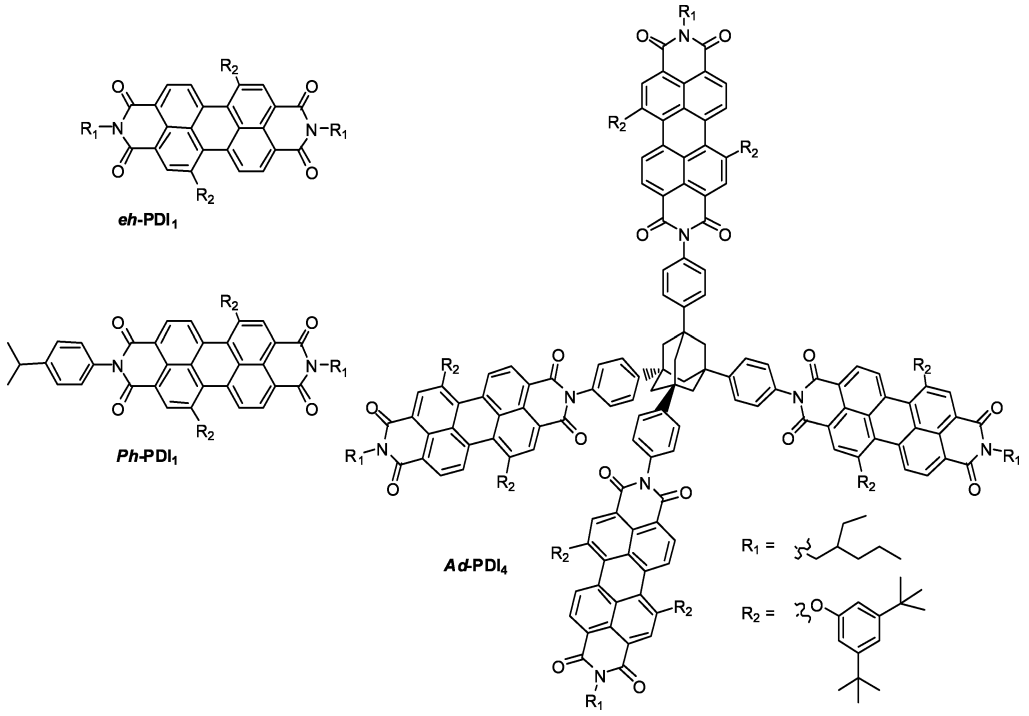

Figure 1. Molecular structures of ***ad*-PDI$_4$**, ***eh*-PDI**, and ***ph*-PDI**.

for the design and development of alternative electron acceptors for OPVs.

Perylene-3,4:9,10-bis(dicarboximide)s (PDIs) offer a number of attractive characteristics as alternatives to fullerenes in OPVs, including favorable orbital energetics, high extinction coefficients in the visible spectral region,[14] photostability,[15] and the capacity to self-assemble into ordered nanostructures.[21,23,24,48] A variety of synthetic strategies have been pursued to prepare different PDI derivatives to test their suitability as OPV electron acceptors.[49,50] These include the incorporation of PDIs into polymers,[51−53] as well as into small donor−acceptor molecules.[54−57] Other strategies, including our own,[58] focused on mitigating detrimental PDI excimer formation as a route to improving charge separation lifetime and solution processing characteristics.[59−61] Previous work incorporated PDIs into dendrimeric or macrocyclic systems that undergo intramolecular energy transfer.[17,25−31,62,63] For example, Langhals et al. synthesized a "star-shaped" tetrahedral PDI tetramer using a tetraphenylmethane core to study the effect of geometric arrangement of the chromophores on their light-harvesting properties. Recently, this compound, which exhibits exceptionally high extinction coefficients,[14,64] was featured in a theoretical study comparing the photophysical properties of a series of symmetric star-shaped versus linear PDI assemblies.[65] Comparing the different PDI geometries, the authors report markedly differing dependencies of oscillator strength distribution on the number of PDI chromophores. They furthermore compare the two bonding motifs as potential light-harvesters in OPV applications and conclude that symmetric assemblies with higher dimensionality would be advantageous, particularly in the solid state, because they will result in a more random distribution of chromophores, which allows for stronger light absorption from numerous incidence angles. A similar tetrahedral PDI tetramer was synthesized for self-assembly studies on gold nanoparticles, wherein the PDI aggregation is inhibited and allows for some control over nanoparticle assembly.[66] Tetrahedral and pyramidal PDI derivatives have also been used to build high surface area porous polyimides for catalysis and gas storage applications.[67] Studies of macrocyclic rings comprising an increasing number of PDI molecules show that ultrafast Förster EET occurs between the PDI molecules and slows somewhat as the ring size increases. This slowing is attributed to greater structural dispersity in the larger, more fluxional rings. Similar work has also been reported using the analogous naphthalene-1,8:4,5-bis(dicarboximide)s (NDIs); for example, fluorescence quenching of the tetrahedral NDI tetramers occurs when they are blended in films with donor polymers.[68] PDI derivatives in which interchromophore $\pi-\pi$ stacking is controlled have now reached 3−4% power conversion efficiency (PCE) in OPVs using polymer donors.[69−72]

We report here a new PDI system that focuses on increasing dimensionality in accordance with a proposed direction for acceptor optimization in an OPV device by attaching four PDI chomophores to a tetraphenyladamantane core (***ad*-PDI$_4$**) to obtain a tetrahedral PDI geometry.[73,74] Ultrafast transient absorption and fluorescence anisotropy measurements show that ultrafast intramolecular EET occurs between adjacent PDI molecules in ***ad*-PDI$_4$**. Furthermore, intermolecular ***ad*-PDI$_4$** aggregation occurs in less polar solvents, such as toluene, leading to more complex EET behavior. Thus, we have developed a PDI acceptor with increased dimensionality and ultrafast, efficient energy-transfer characteristics, which may be a promising acceptor for OPVs.

EXPERIMENTAL SECTION

Synthesis. The synthesis and characterization of ***ad*-PDI$_4$** and model compounds ***ph*-PDI** and ***eh*-PDI** (Figure 1) are detailed in the Supporting Information.

Steady-State Spectroscopy. Steady-state optical absorption measurements were obtained with a Shimadzu 1601 spectrophotometer, and fluorescence measurements were made

dx.doi.org/10.1021/jp500475c | J. Phys. Chem. C XXXX, XXX, XXX−XXX

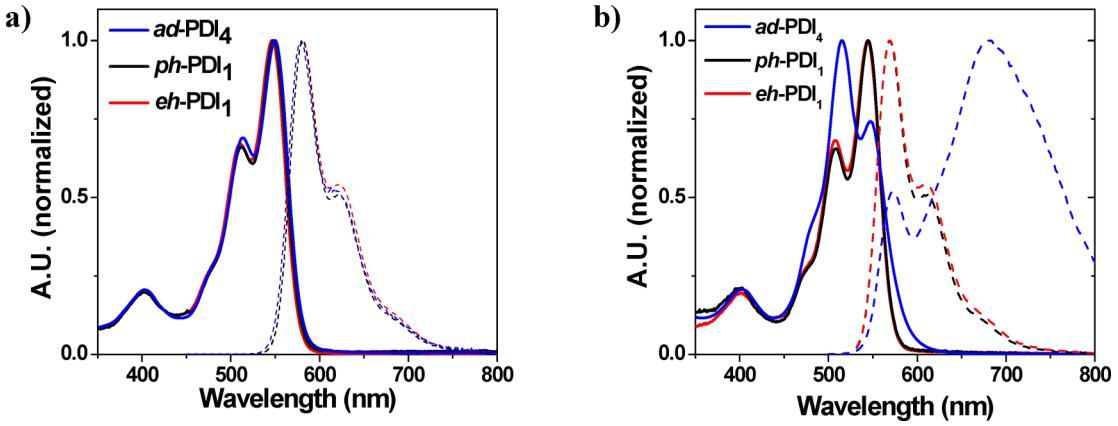

Figure 2. Steady-state absorption (solid) and emission (dashed) spectra of ***ad*-PDI$_4$**, ***ph*-PDI**, and ***eh*-PDI** in (a) CH_2Cl_2 and (b) toluene, normalized to maxima.

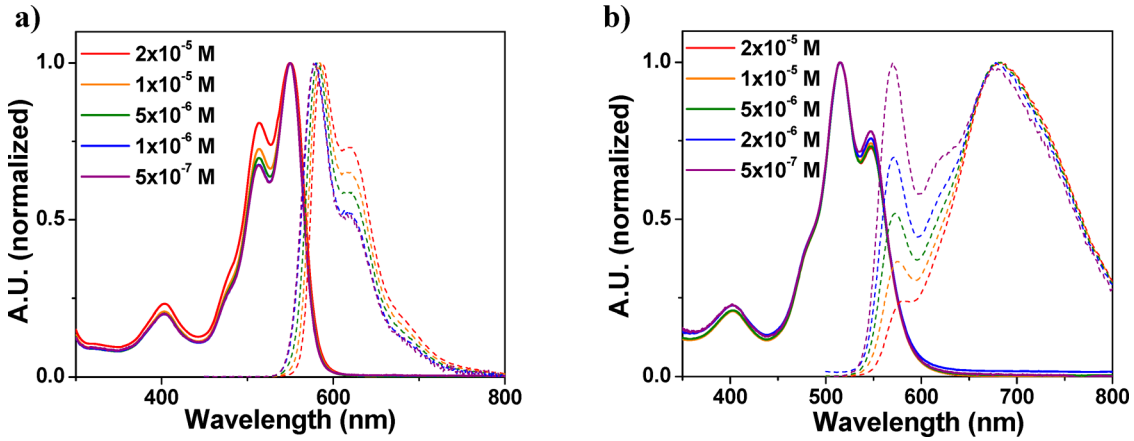

Figure 3. Concentration-dependent steady-state absorption (solid) and emission (dashed) spectra of ***ad*-PDI$_4$** in (a) CH_2Cl_2 and (b) toluene, normalized to the maxima.

with a PT1 Quanta-Master 1 single-photon spectrofluorimeter in a right angle configuration.

Transient Absorption Spectroscopy. Femtosecond transient absorption measurements (fsTA) were made using a home-built Ti:sapphire laser system operating at 2 kHz as detailed previously.[75] The transient spectra were obtained using 3 s of averaging at a given delay time. The pump intensity was varied for the different measurements, as detailed below.

The nanosecond transient absorption (nsTA) apparatus has been described previously;[23] however, the excitation laser used was a Spectra-Physics Lab 150 coupled to a Basiscan OPO (Spectra-Physics). The OPO output was directed to the sample and focused to a beam slightly larger than the probe beam, ensuring efficient pump−probe overlap. One hundred transients were averaged at 5 nm intervals spanning 430 to 800 nm. The transient spectra were constructed by plotting specific time points of each kinetic trace with respect to the corresponding wavelength. Analysis of the kinetic data from both fsTA and nsTA measurements was performed at multiple wavelengths using a Levenberg−Marquardt nonlinear least-squares fit to a general sum-of-exponentials function with a Gaussian convolution to account for the finite instrument response time, which was 150 fs and 7 ns for the fsTA and nsTA setups, respectively.

Time-Resolved Fluorescence and Anisotropy Measurements. Femtosecond time-resolved fluorescence (TRF) was measured by a noncollinear fluorescence up-conversion technique.[76,77] The light source was a home-built cavity-dumped Kerr lens mode-locked Ti:sapphire oscillator pumped by a commercial Nd:YVO_4 laser (Spectra-Physics, Millenia Vs). The center wavelength and spectral width were 830 and 50 nm, respectively. Cavity dumping provided ∼30 nJ pulses at a repetition rate of 820 kHz. Pump pulses at 415 nm were generated by second harmonic generation in a 200 μm thick lithium triborate (LBO) crystal. The residual fundamental was used as a gate pulse in the fluorescence up-conversion. Pairs of fused-silica prisms compensate for the group velocity dispersion of the pump and gate pulses.

For the time-resolved fluorescence anisotropy measurements, polarization of the pump pulse was rotated with respect to the gate pulse by using a $\lambda/2$ waveplate. A singlet lens of f = 5 cm was used to focus the pump beam into the 200 μm path-length cuvette. Fluorescence was collected by a reflective objective and mixed with the gate pulse in a 500 μm thick BBO crystal. The up-conversion signal was sent to a counter (SR400, Stanford Research Systems). The instrument response was estimated to be 100 fs from the cross-correlation between the scattered pump and gate pulses. Emission anisotropy decays were calculated using eq 1.

$$r(t) = \frac{I_{\parallel}(t) - I_{\perp}(t)}{I_{\parallel}(t) + 2I_{\perp}(t)} \quad (1)$$

dx.doi.org/10.1021/jp500475c | J. Phys. Chem. C XXXX, XXX, XXX−XXX

Picosecond time-resolved fluorescence measurements were made using a streak camera system (Hamamatsu C4780 Streakscope). A parabolic mirror was used to focus the excitation beam into the sample, and the subsequent fluorescence was collected in a backscattering geometry using the same parabolic mirror. Magic angle detection was used to avoid polarization effects. The IRF was 750 ps in a 50 ns time window. All data were acquired in single-photon counting mode using the Hamamatsu HPD-TA software.

RESULTS

Steady-State Characterization. The steady-state optical absorption and fluorescence spectra of ***ad*-PDI$_4$** and model compounds ***ph*-PDI** and ***eh*-PDI** in CH_2Cl_2 and toluene are shown in Figure 2. The steady-state characteristics in CH_2Cl_2 are very similar for all three molecules, with absorption across 350−600 nm and maxima at 550 nm. The fluorescence spans 550−750 nm, and the emission maxima are at 585 nm. In toluene, the model compounds exhibit steady-state characteristics very similar to those in CH_2Cl_2, with the absorption and fluorescence maxima shifted to 555 and 575 nm, respectively. The absorption of ***ad*-PDI$_4$** in toluene still spans 350−800 nm, but the maximum is at 520 nm, representing a large blue-shift relative to the same molecule in CH_2Cl_2, as well as a line shape change. The fluorescence spectrum of ***ad*-PDI$_4$** in toluene also shows a line shape change, with a broad peak with maximum at 670 nm and a significant but smaller peak at 575 nm.

Concentration-dependent absorption and fluorescence measurements of ***ad*-PDI$_4$** in CH_2Cl_2 and toluene are shown in Figure 3. The spectra are normalized for comparison; non-normalized spectra can be found in Figure S1 of the Supporting Information. At higher concentrations in CH_2Cl_2, the relative ratios of the peak heights at 510 and 550 nm begin to switch in both the absorption and fluorescence. The normalized traces in toluene demonstrate that the absorption line shape does not change significantly with varying concentration. However, in the fluorescence spectrum, the peak at 575 nm decreases in relative intensity with increasing concentration, while the broad peak at 670 nm maintains a persistent peak position and line shape. The molar extinction coefficient of ***ad*-PDI$_4$** was measured at low concentrations in CH_2Cl_2 and found to be 215 000 M^{-1} cm^{-1}. Incorporation of PDI into ***ad*-PDI$_4$** does not change its reduction potential ($E_{1/2}$ = −0.54 V vs SCE) relative to that of the monomer.[78]

Transient Absorption Spectroscopy. FsTA measurements of ***ad*-PDI$_4$**, ***ph*-PDI**, and ***eh*-PDI** were performed in CH_2Cl_2 at 532 nm excitation using 150 fs pulses and are shown in Figures 4, 5, and S2 of the Supporting Information, respectively. All three molecules exhibit negative ΔA features from 450 to 650 nm, attributable to ground-state bleach (GSB) and stimulated emission (SE), and a positive feature centered around 700 nm, which is attributed to the singlet excited-state PDI absorption (^{1}*PDI). The decay of ^{1}*PDI was monitored by recovery of the SE at 575 nm. In the model compounds this decay fits to monoexponential kinetics of τ = 5.0 and 5.8 ns for ***ph*-PDI** and ***eh*-PDI**, respectively (Table 1). In ***ad*-PDI$_4$**, the SE exhibits biexponential kinetics with τ_1 = 12 ps and τ_2 = 4.4 ns (Table 1). Furthermore, the relative amplitude of two lifetimes found in ***ad*-PDI$_4$** is laser intensity-dependent (Figure 4, inset). No formation of a long-lived triplet state is observed as is consistent with the very low triplet yields of PDI monomers.[79]

The transient spectra of ***ph*-PDI** and ***eh*-PDI** in toluene (Figures S3 and S4 of the Supporting Information, respectively)

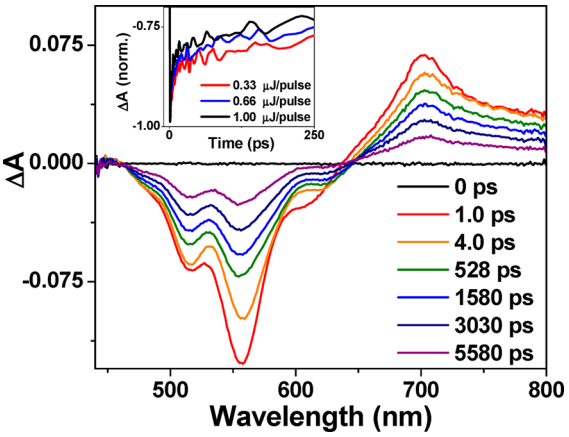

Figure 4. FsTA of ***ad*-PDI$_4$** in CH_2Cl_2 at 532 nm; inset shows the laser power dependence of the transient kinetics monitored at 575 nm, which show increasing singlet annihilation with increasing incident pump power.

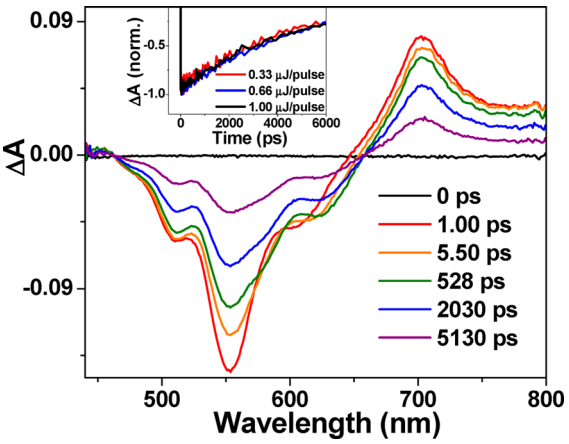

Figure 5. FsTA of ***ph*-PDI** in CH_2Cl_2 at λ_{ex} = 532 nm; inset shows the power dependence of the transient kinetics monitored at 575 nm, which do not display any significant changes with increasing incident pump power.

Table 1. Kinetic Decay Lifetimes for *ad*-PDI$_4$ and Model Compounds in CH_2Cl_2

	TA[a]		TRF[b]
compound	ps	ns	ns
***ph*-PDI**	–	5.8 ± 0.2	5.1 ± 0.1
***eh*-PDI**	–	5.0 ± 0.1	5.3 ± 0.1
***ad*-PDI$_4$**	12 ± 1	4.4 ± 0.1	4.6 ± 0.1

[a]Probed at 575 nm. [b]Probed at 585 nm.

show features very similar to those in CH_2Cl_2, while the transient decay kinetics are again monoexponential, with τ = 4.7 and 4.5 ns for ***ph*-PDI** and ***eh*-PDI**, respectively (Table 2). FsTA spectra of ***ad*-PDI$_4$** in toluene (Figure 6a) exhibit negative features from 450 to 550 nm, which are attributed to GSB. Also evident is an absorptive feature, which extends from 600 to 800 nm. Furthermore, there is no evidence of SE in the transient spectrum. The transient kinetics, probed within the GSB at 550 nm, exhibit a fast decay, followed by a second component, which lives beyond the 5 ns resolution of the fsTA apparatus; thus, ***ad*-PDI$_4$** in toluene was also studied using nanosecond transient absorption spectroscopy. The nsTA

dx.doi.org/10.1021/jp500475c | J. Phys. Chem. C XXXX, XXX, XXX−XXX

Table 2. Kinetic Decay Lifetimes for *ad*-PDI$_4$ and Model Compounds in Toluene

	TA		TRF	
compound	ps	ns	ns	ns
***ph*-PDI**	–	4.7 ± 0.1[a]	4.76 ± 0.04[a]	–
***eh*-PDI**	–	4.5 ± 0.1[a]	5.05 ± 0.04[a]	–
***ad*-PDI$_4$**	2.1 ± 0.5[b] (0.15)	28 ± 1[b] (0.85)	4.34 ± 0.04[a]	–
			7.1 ± 1.7[c]	30 ± 1[c]

[a]Probed at 575 nm. [b]Probed at 585 nm. [c]Probed at 670 nm.

spectra (Figure 6b) demonstrate spectral features that are the same as those of the fsTA spectra, and transient kinetics probed at 550 nm fit to a monoexponential lifetime. Thus, the combined fsTA and nsTA results show that the ***ad*-PDI$_4$** excited-state dynamics in toluene decay biexponentially with τ_1 = 2.1 ps and τ_2 = 28 ns (Table 2). FsTA and nsTA measurements were repeated at λ_{ex} = 416 nm and yielded results very similar to those with λ_{ex} = 532 nm (Figures S5–S10 and Table S1 of the Supporting Information). The excited-state dynamics are therefore excitation wavelength-independent. A small amount of long-lived triplet state is observed as is characteristic of PDI dimers and higher oligomers.[78,80]

Time-Resolved Fluorescence Measurements. Picosecond time-resolved fluorescence (psTRF) measurements of ***ad*-PDI$_4$**, ***ph*-PDI**, and ***eh*-PDI** in CH_2Cl_2 and toluene were performed using λ_{ex} = 416 nm. The resulting fluorescence decays in CH_2Cl_2 are all monoexponential (Figure S11 of the Supporting Information). The fast decay component observed in the ***ad*-PDI$_4$** spectra is not visible within the 750 ps instrument resolution of the psTRF apparatus. Thus, the psTRF and fsTA measurements in CH_2Cl_2 are in reasonable agreement (Table 1).

PsTRF measurements of ***ph*-PDI** and ***eh*-PDI** in toluene also show monoexponential decays in agreement with those observed by fsTA (Figure S12 of the Supporting Information). ***Ad*-PDI$_4$** in toluene exhibits two fluorescence peaks, as discussed above (Figure 2b). Fluorescence kinetics probed at 575 nm decay monoexponentially with τ = 4.34 ns. The fluorescence signal probed at 670 nm, however, fits to a biexponential decay with τ_1 = 7.1 and τ_2 = 30 ns (Table 2 and Figure S12 of the Supporting Information).

Transient Fluorescence Anisotropy Measurements. To further explore the nature of the picosecond decay component observed in the fsTA data of ***ad*-PDI$_4$**, transient fluorescence anisotropy was measured in CH_2Cl_2 and toluene for both ***ad*-PDI$_4$** (Figure 7) and ***ph*-PDI** (Figure S13 of the Supporting Information). The anisotropy decay constants are summarized in Table 3. The differences between the depolarization dynamics of ***ad*-PDI$_4$** and ***ph*-PDI** and the implications therein are discussed in detail below.

DISCUSSION

Monomeric and Aggregated *ad*-PDI$_4$. ***Ad*-PDI$_4$** exhibits solvent-dependent steady-state photophysics. In CH_2Cl_2 solution, this molecule closely resembles the model compounds at low concentrations and most likely contains predominantly ***ad*-PDI$_4$** monomers. The ***ad*-PDI$_4$** 215 000 M^{-1} cm^{-1} extinction coefficient is physically reasonable because that of the ***eh*-PDI** monomer is 46 000 M^{-1} cm^{-1}.[16] However, at higher ***ad*-PDI$_4$** concentrations in CH_2Cl_2 solution, the relative peak intensities of the 0–0 and the 0–1 vibronic bands invert. This effect is much more pronounced in toluene solution, where the absorption spectrum maximum is strongly blue-shifted, and is indicative of PDI *H*-aggregate formation.[16,81,82] Such an interaction can occur only intermolecularly between ***ad*-PDI$_4$** molecules because intramolecular PDI stacking interactions are precluded by the ***ad*-PDI$_4$** molecular structure. This intermolecular interaction is strongly concentration-dependent.

The ***ad*-PDI$_4$** steady-state emission spectrum in toluene is characterized by a broad, featureless emission centered at 670 nm, which is typical of excimer fluorescence.[16,19] There remains, however, a shoulder at 575 nm, where PDI monomer fluorescence is observed, and the intensity of this shoulder decreases with increasing concentration. Thus, it is clear that the number of PDI molecules that π-stack with neighboring molecules is concentration-dependent but does not appear to reach a limit within the range measured. The steady-state spectra suggest that at high concentrations in toluene, the ***ad*-PDI$_4$** system may be forming a large-scale, three-dimensional network through intermolecular *H*-aggregation. Attempts were made to characterize macromolecular aggregate size and shape using solution-phase small- and wide-angle X-ray scattering (SAXS/WAXS).[7,20,83–85] No distinct size was resolved, indicating that there is a broad distribution of aggregate sizes.

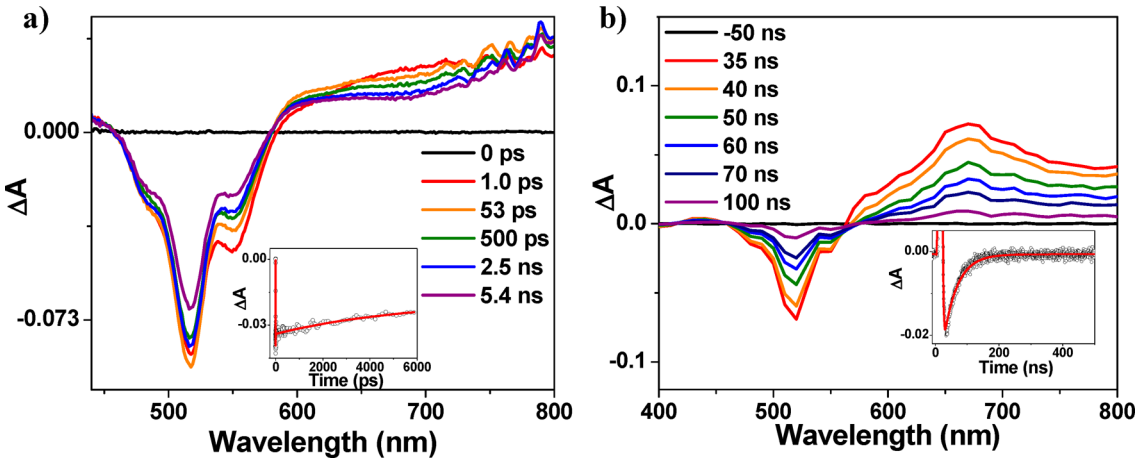

Figure 6. (a) Femtosecond TA and (b) nanosecond TA of ***ad*-PDI$_4$** in toluene at λ_{ex} = 532 nm; inset shows the transient kinetics monitored at 550 nm.

dx.doi.org/10.1021/jp500475c | J. Phys. Chem. C XXXX, XXX, XXX–XXX

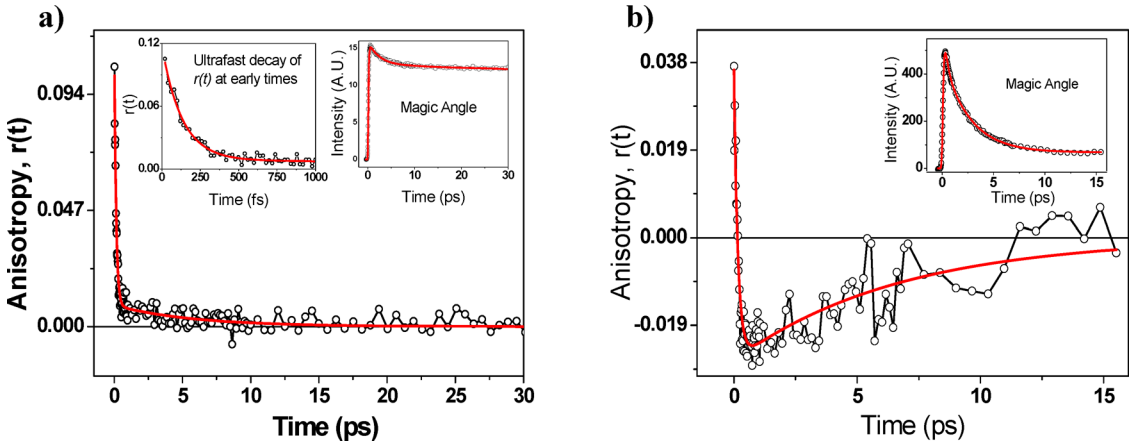

Figure 7. Time-resolved fluorescence anisotropy of ***ad*-PDI$_4$** in (a) CH_2Cl_2 and (b) toluene at λ_{ex} = 415 nm. Insets show kinetic decay at magic-angle detection.

Table 3. Kinetic Analysis of Transient Fluorescence Anisotropy Measurements at 575 nm

	CH_2Cl_2		toluene	
compound	τ_R (fs)	τ_D (ps)	τ_R (fs)	τ_D (ps)
***ph*-PDI**	137 ± 41 fs	158 ± 30 ps	68 ± 14 fs	186 ± 45 ps
***ad*-PDI$_4$**	131 ± 12 fs	6 ± 2 ps	158 ± 72 fs	7 ± 4 ps

Considering the tetrahedral symmetry of ***ad*-PDI$_4$**, there is in fact no a priori limit to the size of the intermolecular network. When incorporating PDI acceptors into OPVs is attempted, numerous reports have commented on the importance of optimal balance between solubility and π-stacking of the PDIs.[69−72] The formation of intermolecular stacked structures is potentially beneficial for creating well-connected acceptor domains in films. However, these aggregated structures can also form disconnected trap sites and detrimental film morphologies due to insolubility. The ability of ***ad*-PDI$_4$** to form intermolecular aggregates that are still soluble speaks to an advantage of this molecular architecture. In addition, the variability of aggregate size suggests that in solution-processed films, particularly when paired with a donor molecule or polymer, ***ad*-PDI$_4$** packing can be a tunable parameter to find the most suitable concentration of monomers and/or aggregates.

EET within Monomeric *ad*-PDI$_4$. Transient absorption spectroscopy and fluorescence lifetime measurements on ***ad*-PDI$_4$** in CH_2Cl_2 solution exhibit biexponential recovery kinetics, whereas the model compounds exhibit monoexponential recovery kinetics (Table 1). The model compounds behave quite similarly despite differing imide substituents. Therefore, the change in ***ad*-PDI$_4$** behavior relative to these reference molecules is not due to asymmetric imide substitution. The short decay component of the biexponential kinetics of ***ad*-PDI$_4$** is laser intensity-dependent. This component is attributed to singlet−singlet annihilation.[5,8,31,48] In multichromophore arrays, in which the chromophores have large extinction coefficients, two or more chromophores can be excited at typical femtosecond laser photon fluences. Rapid EET of these singlet excitons (S_1 states) within the array can result in two excitons colliding. This collision may result in destruction of one exciton as a consequence of one chromophore being promoted to a higher S_n state, while the other chromophore simultaneously decays nonradiatively to its ground S_0 state. The statistical likelihood of observing annihilation due to EET within a chromophore array depends on the number of excited chromophores, which in turn depends on laser intensity. Thus, the laser intensity-dependent fast component observed in the ***ad*-PDI$_4$** monomer in CH_2Cl_2 solution suggests that rapid excitation energy transfer is occurring within this multichromophore system.

The EET hypothesis was further probed using femtosecond transient fluorescence anisotropy measurements.[86,87] This technique monitors the temporal characteristics of the transition dipole moment direction following photoexcitation. Upon EET to an adjacent chromophore, the change in excited transition dipole moment direction can be related to the EET rate between the chromophores. Such anisotropy measurements also reveal decay features due to rotational diffusion, which is usually canceled out using measurements at the magic angle. To analyze the anisotropy data, the rotational diffusion time constant of the model ***ph*-PDI** was estimated using the modified Stokes−Debye−Einstein relationship

$$\tau_{rot} = \frac{\eta V}{k_B T} \times f \tag{2}$$

where η is the viscosity of the solvent, V the hydrodynamic volume of the rotating unit, and k_B the Boltzmann constant, T the temperature, and f the shape factor as determined from Perrin's equation for a hydrodynamic ellipsoid (eq 3),[88] where p is the axial ratio of the molecule and is calculated as 1.25 for ***ph*-PDI**.

$$f_\perp = \frac{2}{3}\frac{p[(2p^2 - 1)S - p]}{p^4 - 1}$$
$$S = (p^2 - 1)^{-1/2} \ln[p + (p^2 - 1)^{1/2}] \tag{3}$$

V is determined from an MM+ energy-optimized structure and is 1.002 × 10^{-30} m^3 for ***ph*-PDI**. The calculated rotational diffusion time for the model molecule is therefore 130 ps in CH_2Cl_2. The measured anisotropy decay of ***ph*-PDI** in CH_2Cl_2

dx.doi.org/10.1021/jp500475c | J. Phys. Chem. C XXXX, XXX, XXX−XXX

gave a rise time of 137 ± 41 fs, which is attributed to internal conversion from S_2 to S_1, and a decay time of 158 ± 30 ps, which agrees well with the calculated τ_{rot}. Analysis of the anisotropy data for ***ad*-PDI$_4$** in CH_2Cl_2 solution gives a rise time of 131 ± 12 fs, which is again attributed to internal conversion, and a decay time of 6 ± 2 ps, which is attributed to EET between neighboring PDI chromophores in the ***ad*-PDI$_4$** molecule.

The theoretical Förster EET rate was calculated using eq 4 to elucidate the mechanism of energy transfer within the ***ad*-PDI$_4$** monomer.[89]

$$k_{EET} = \frac{\varphi_D \kappa^2}{\tau_D r^6}\left(\frac{9000(\ln 10)}{128\pi^5 N \eta^4}\right)\int_0^\infty F_D(\lambda)\varepsilon_A(\lambda)\lambda^4\, d\lambda \quad (4)$$

Here, κ^2 is the orientation factor, ϕ_D the donor fluorescence quantum yield in the absence of the acceptor, n^2 the refractive index of the solvent, N Avogadro's number, r the distance between the donor and acceptor, τ_D the fluorescence lifetime of the donor, $F_D(\lambda)$ the fluorescence intensity of the donor normalized to unity, λ the wavelength, and ε_A the extinction coefficient of the acceptor. In this case, the ***ph*-PDI** spectra were used for both donor and acceptor, where the fluorescence quantum yield of ***ph*-PDI** is 0.98 and its fluorescence lifetime is 5.1 ns (Table 1). The MM+ energy-optimized structure of ***ad*-PDI$_4$** yields a value of 21 Å for R and an orientation factor of $\kappa^2 = 2.77$ based on the fixed orientation of the PDI-PDI transition dipole moments within ***ad*-PDI$_4$**. Using these data, eq 4 yields a calculated Förster energy-transfer time constant of $\tau_{EET} = 5.9$ ps within ***ad*-PDI$_4$**. This time constant agrees very well with the measured value of 6 ps (transient anisotropy data) and suggests that there is no significant contribution from overlap-driven Dexter energy transfer. This is reasonable given that there are five saturated bonds and two phenyl groups between any two PDI molecules, and both the HOMO and LUMO of PDI have nodal planes that bisect the N−N axis, limiting electronic coupling between the PDI and the spacer.

Previous work on PDI-based dendrimers and macrocycles reported EET characteristics which were well-described by Förster theory for the more rigid first generations and for smaller macrocylic rings. However, with increasing size and structural flexibility, there is increased energetic disorder, so that the predictions of Förster theory become less reliable.[31,62,63] In contrast, the fixed tetrahedral geometric relationship between the PDI transition moments within ***ad*-PDI$_4$** results in a closer match between the measured EET rate and the predictions of Förster theory.

Excimer Formation and EET in Toluene. The fsTA and nsTA spectra of ***ad*-PDI$_4$** in toluene solution exhibit broad positive features, and the nsTA and TRF data show that excited-state decay occurs with $\tau = 30$ ns, in agreement with our previous studies of the excited-state lifetimes of discrete PDI *H*-aggregates.[16] This longer lifetime is attributed to the formation of an excimer state, in agreement with the steady-state spectroscopic characterization, which suggests that intermolecular ***ad*-PDI$_4$** aggregates form in toluene. Describing EET processes in these aggregates is difficult because $\pi-\pi$ stacking between PDIs on adjacent tetramers undoubtedly leads to aggregated networks of widely varying size as indicated by the inability of SAX/WAXS measurements to determine a definite size. Furthermore, not all of the PDIs are participating in stacking interactions. Thus, ***ad*-PDI$_4$** retains some monomeric fluorescence features, ensuring retention of the spectral overlap required for Förster EET.[90] The fluorescence anisotropy of ***ad*-PDI$_4$** in toluene reveals a 158 ± 72 fs component, attributable to internal conversion from S_2 to S_1, and then a 7 ± 4 ps rise, which is in agreement with the EET rate for the molecule in CH_2Cl_2 solution. It is therefore reasonable that the EET rate should be the same for the monomer and the aggregated system because the observed time constant reflects the short distance intramolecular EET.

CONCLUSIONS

The goal of this work is to probe the photophysical properties of the tetrahedral molecule ***ad*-PDI$_4$**, a PDI-based electron acceptor with high symmetry, which mimics benchmark fullerene-based acceptors that have been credited with facilitating efficient packing and intermolecular energy and charge transfer in OPV films. Time-resolved fluorescence anisotropy measurements in CH_2Cl_2 solution show that PDI−PDI EET occurs in $\tau = 6$ ps. Furthermore, this tetrahedral structure forms a network of intermolecular aggregates in toluene solution having the same EET time constants, which suggests that ***ad*-PDI$_4$** may be an interesting potential replacement for fullerene-based acceptors in OPVs.

ASSOCIATED CONTENT

Supporting Information

Experimental details including synthesis and further spectroscopic data as described in the text. This material is available free of charge via the Internet at http://pubs.acs.org.

AUTHOR INFORMATION

Corresponding Author

*E-mail: m-wasielewski@northwestern.edu.

Notes

The authors declare no competing financial interest.

ACKNOWLEDGMENTS

Synthesis (CR) was supported by the Office of Naval Research under Grant N00014-05-1-0021 (M.R.W.) and BP Solar, Inc. (T.J.M., M.R.W.). Spectroscopy (C.R., C.H.K., T.J.M., M.R.W.) was supported as part of the ANSER Center, an Energy Frontier Research Center funded by the U.S. Department of Energy, Office of Science, Office of Basic Energy Sciences, under Award DE-SC0001059. NMR and MS measurements were carried out at the Integrated Molecular Structure Education and Research Center (IMSERC) at Northwestern University. C.R. thanks Dr. Amanda L. Smeigh for help with nanosecond transient absorption experiments and Dr. Kelly M. Lefler for the SAXS experiments and helpful discussions.

REFERENCES

(1) Blankenship, R. E. *Molecular Mechanisms of Photosynthesis*; Blackwell Science: Oxford, U.K., 2002.

(2) Wasielewski, M. R. Self-Assembly Strategies for Integrating Light Harvesting and Charge Separation in Artificial Photosynthetic Systems. *Acc. Chem. Res.* **2009**, *42*, 1910−1921.

(3) Wasielewski, M. R. Photoinduced Electron Transfer in Supramolecular Systems for Artificial Photosynthesis. *Chem. Rev.* **1992**, *92*, 435−461.

(4) Gunderson, V. L.; Conron, S. M. M.; Wasielewski, M. R. Self-Assembly of a Hexagonal Supramolecular Light-Harvesting Array from Chlorophyll *a* Trefoil Building Blocks. *Chem. Commun. (Cambridge, U.K.)* **2010**, *46*, 401−403.

(5) Gunderson, V. L.; Wilson, T. M.; Wasielewski, M. R. Excitation Energy Transfer Pathways in Asymmetric Covalent Chlorophyll *a* Tetramers. *J. Phys. Chem. C* **2009**, *113*, 11936−11942.
(6) Kelley, R. F.; Tauber, M. J.; Wasielewski, M. R. Linker-Controlled Energy and Charge Transfer within Chlorphyll Trefoils. *Angew. Chem., Int. Ed.* **2006**, *45*, 7979−7982.
(7) Mickley Conron, S. M.; Shoer, L. E.; Smeigh, A. L.; Ricks, A. B.; Wasielewski, M. R. Photoinitiated Electron Transfer in Zinc Porphyrin−Perylenediimide Cruciforms and Their Self-Assembled Oligomers. *J. Phys. Chem. B* **2013**, *117*, 2195−2204.
(8) Kelley, R. F.; Goldsmith, R. H.; Wasielewski, M. R. Ultrafast Energy Transfer within Cyclic Self-Assembled Chlorophyll Tetramers. *J. Am. Chem. Soc.* **2007**, *129*, 6384−6385.
(9) Hindin, E.; Forties, R. A.; Loewe, R. S.; Ambroise, A.; Kirmaier, C.; Bocian, D. F.; Lindsey, J. S.; Holten, D.; Knox, R. S. Excited-State Energy Flow in Covalently Linked Multiporphyrin Arrays: The Essential Contribution of Energy Transfer between Nonadjacent Chromophores. *J. Phys. Chem. B* **2004**, *108*, 12821−12832.
(10) Song, H.-e.; Kirmaier, C.; Schwartz, J. K.; Hindin, E.; Yu, L.; Bocian, D. F.; Lindsey, J. S.; Holten, D. Mechanisms, Pathways, and Dynamics of Excited-State Energy Flow in Self-Assembled Wheel-and-Spoke Light-Harvesting Architectures. *J. Phys. Chem. B* **2006**, *110*, 19121−19130.
(11) El-Khouly, M. E.; Kim, J. H.; Kay, K.-Y.; Choi, C. S.; Ito, O.; Fukuzumi, S. Synthesis and Photoinduced Intramolecular Processes of Light-Harvesting Silicon Phthalocyanine−Naphthalenediimide−Fullerene Connected Systems. *Chem.—Eur. J.* **2009**, *15*, 5301−5310.
(12) Berera, R.; van Stokkum, I. H. M.; Kodis, G.; Keirstead, A. E.; Pillai, S.; Herrero, C.; Palacios, R. E.; Vengris, M.; van Grondelle, R.; Gust, D.; et al. Energy Transfer, Excited-State Deactivation, and Exciplex Formation in Artificial Caroteno-Phthalocyanine Light-Harvesting Antennas. *J. Phys. Chem. B* **2007**, *111*, 6868−6877.
(13) Li, X.; Sinks, L. E.; Rybtchinski, B.; Wasielewski, M. R. Ultrafast Aggregate-to-Aggregate Energy Transfer within Self-Assembled Light-Harvesting Columns of Zinc Phthalocyanine Tetrakis-(Perylenediimide). *J. Am. Chem. Soc.* **2004**, *126*, 10810−10811.
(14) Langhals, H. Control of the Interactions in Multichromophores: Novel Concepts. Perylene Bis-Imides as Components for Larger Functional Units. *Helv. Chim. Acta* **2005**, *88*, 1309−1343.
(15) Würthner, F. Perylene Bisimide Dyes as Versatile Building Blocks for Functional Supramolecular Architectures. *Chem. Commun. (Cambridge, U.K.)* **2004**, 1564−1579.
(16) Giaimo, J. M.; Lockard, J. V.; Sinks, L. E.; Scott, A. M.; Wilson, T. M.; Wasielewski, M. R. Excited Singlet States of Covalently Bound, Cofacial Dimers and Trimers of Perylene-3,4:9,10-Bis(Dicarboximide). *J. Phys. Chem. A* **2008**, *112*, 2322−2330.
(17) Hippius, C.; Schlosser, F.; Vysotsky, M. O.; Boehmer, V.; Würthner, F. Energy Transfer in Calixarene-Based Cofacial-Positioned Perylene Bisimide Arrays. *J. Am. Chem. Soc.* **2006**, *128*, 3870−3871.
(18) Rybtchinski, B.; Sinks, L. E.; Wasielewski, M. R. Photoinduced Electron Transfer in Self-Assembled Dimers of Three-Fold Symmetric Donor-Acceptor Molecules Based on Perylene-3,4:9,10-Bis-(Dicarboximide). *J. Phys. Chem. A* **2004**, *108*, 7497−7505.
(19) Langhals, H.; Ismael, R. Cyclophanes as Model Compounds for Permanent, Dynamic Aggregates. Induced Chirality with Strong Cd Effects. *Eur. J. Org. Chem.* **1998**, 1915−1917.
(20) Lefler, K. M.; Co, D. T.; Wasielewski, M. R. Self-Assembly-Induced Ultrafast Photodriven Charge Separation in Perylene-3,4-Dicarboximide-Based Hydrogen-Bonded Foldamers. *J. Phys. Chem. Lett.* **2012**, *3*, 3798−3805.
(21) Thalacker, C.; Würthner, F. Chiral Perylene Bisimide-Melamine Assemblies: Hydrogen Bond-Directed Growth of Helically Stacked Dyes with Chiroptical Properties. *Adv. Funct. Mater.* **2002**, *12*, 209−218.
(22) Würthner, F.; Thalacker, C.; Sautter, A. Hierarchical Organization of Functional Perylene Chromophores to Mesoscopic Superstructures by Hydrogen Bonding and $\pi-\pi$ Interactions. *Adv. Mater.* **1999**, *11*, 754−758.
(23) Bullock, J. E.; Carmieli, R.; Mickley, S. M.; Vura-Weis, J.; Wasielewski, M. R. Photoinitiated Charge Transport Through π-Stacked Electron Conduits in Supramolecular Ordered Assemblies of Donor−Acceptor Triads. *J. Am. Chem. Soc.* **2009**, *131*, 11919−11929.
(24) van der Boom, T.; Hayes, R. T.; Zhao, Y.; Bushard, P. J.; Weiss, E. A.; Wasielewski, M. R. Charge Transport in Photofunctional Nanoparticles Self-Assembled from Zinc 5,10,15,20-Tetrakis(Perylene-Diimide)Porphyrin Building Blocks. *J. Am. Chem. Soc.* **2002**, *124*, 9582−9590.
(25) Cotlet, M.; Vosch, T.; Habuchi, S.; Weil, T.; Müllen, K.; Hofkens, J.; De Schryver, F. Probing Intramolecular Förster Resonance Energy Transfer in a Naphthaleneimide−Peryleneimide−Terrylenediimide-Based Dendrimer by Ensemble and Single-Molecule Fluorescence Spectroscopy. *J. Am. Chem. Soc.* **2005**, *127*, 9760−9768.
(26) De Schryver, F. C.; Maus, M.; De, R.; Lor, M.; Weil, T.; Mitra, S.; Wiesler, U. M.; Herrmann, A.; Hofkens, J.; Vosch, T.; et al. Intramolecular Energy Hopping and Energy Trapping in Polyphenylene Dendrimers with Multiple Peryleneimide Donor Chromophores and a Terryleneimide Acceptor Trap Chromophore. *J. Am. Chem. Soc.* **2001**, *123*, 7668−7676.
(27) Fron, E.; Pilot, R.; Schweitzer, G.; Qu, J. Q.; Herrmann, A.; Müllen, K.; Hofkens, J.; van der Auweraer, M.; De Schryver, F. C. Photoinduced Electron-Transfer in Perylenediimide Triphenylamine-Based Dendrimers: Single Photon Timing and Femtosecond Transient Absorption Spectroscopy. *Photochem. Photobiol. Sci.* **2008**, *7*, 597−604.
(28) Hofkens, J.; Maus, M.; Gensch, T.; Vosch, T.; Cotlet, M.; Koehn, F.; Herrmann, A.; Müllen, K.; De Schryver, F. Probing Photophysical Processes in Individual Multichromophoric Dendrimers by Single-Molecule Spectroscopy. *J. Am. Chem. Soc.* **2000**, *122*, 9278−9288.
(29) Qu, J. Q.; Pschirer, N. G.; Liu, D. J.; Stefan, A.; De Schryver, F. C.; Müllen, K. Dendronized Perylenetetracarboxdiimides with Peripheral Triphenylamines for Intramolecular Energy and Electron Transfer. *Chem.—Eur. J.* **2004**, *10*, 528−537.
(30) Schweitzer, G.; Gronheid, R.; Jordens, S.; Lor, M.; Belder, G. D.; Weil, T.; Reuther, E.; Müllen, K.; Schyver, F. C. D. Intramolecular Directional Energy Transfer Processes in Dendrimers Containing Perylene and Terrylene Chromophores. *J. Phys. Chem. A* **2003**, *107*, 3199−3207.
(31) Vosch, T.; Cotlet, M.; Hofkens, J.; Van der Biest, K.; Lor, M.; Weston, K.; Tinnefeld, P.; Sauer, M.; Latterini, L.; Müllen, K.; et al. Probing Förster Type Energy Pathways in a First Generation Rigid Dendrimer Bearing Two Perylene Imide Chromophores. *J. Phys. Chem. A* **2003**, *107*, 6920−6931.
(32) Anthony, J. E. Small-Molecule, Nonfullerene Acceptors for Polymer Bulk Heterojunction Organic Photovoltaics. *Chem. Mater.* **2011**, *23*, 583−590.
(33) Delgado, J. L.; Bouit, P. A.; Filippone, S.; Herranz, M. A.; Martin, N. Organic Photovoltaics: A Chemical Approach. *Chem. Commun. (Cambridge, U.K.)* **2010**, *46*, 4853−4865.
(34) Collini, E.; Wong, C. Y.; Wilk, K. E.; Curmi, P. M. G.; Brumer, P.; Scholes, G. D. Coherently Wired Light-Harvesting in Photosynthetic Marine Algae at Ambient Temperature. *Nature* **2010**, *463*, 644−U669.
(35) Kim, M. H.; Cho, M. J.; Kim, K. H.; Hoang, M. H.; Lee, T. W.; Jin, J. I.; Kang, N. S.; Yu, J. W.; Choi, D. H. Organic Donor-σ-Acceptor Molecules Based on 1,2,4,5-Tetrakis((E)-2-(5′-Hexyl-2,2′-Bithiophen-5-yl)Vinyl)Benzene and Perylene Diimide Derivative and Their Application to Photovoltaic Devices. *Org. Electron.* **2009**, *10*, 1429−1441.
(36) Liang, F. S.; Lu, J. P.; Ding, J. F.; Movileanu, R.; Tao, Y. Design and Synthesis of Alternating Regioregular Oligothiophenes/Benzothiadiazole Copolymers for Organic Solar Cells. *Macromolecules* **2009**, *42*, 6107−6114.
(37) Troshin, P. A.; Koeppe, R.; Susarova, D. K.; Polyakova, N. V.; Peregudov, A. S.; Razumov, V. F.; Sariciftci, N. S.; Lyubovskaya, R. N. Trannulenes: A New Class of Photoactive Materials for Organic Photovoltaic Devices. *J. Mater. Chem.* **2009**, *19*, 7738−7744.

(38) Tang, C. W. Two-Layer Organic Photovoltaic Cell. *Appl. Phys. Lett.* **1986**, *48*, 183−185.
(39) Forrest, S. R. The Limits to Organic Photovoltaic Cell Efficiency. *MRS Bull.* **2005**, *30*, 28−32.
(40) Kippelen, B.; Bredas, J.-L. Organic Photovoltaics. *Energy Environ. Sci.* **2009**, *2*, 251−261.
(41) Janssen, R. A. J.; Nelson, J. Factors Limiting Device Efficiency in Organic Photovoltaics. *Adv. Mater.* **2013**, *25*, 1847−1858.
(42) Würthner, F.; Meerholz, K. Systems Chemistry Approach in Organic Photovoltaics. *Chem.—Eur. J.* **2010**, *16*, 9366−9373.
(43) Zhu, X. Y.; Kahn, A. Electronic Structure and Dynamics at Organic Donor/Acceptor Interfaces. *MRS Bull.* **2010**, *35*, 443−448.
(44) Yi, Y. P.; Coropceanu, V.; Bredas, J. L. Exciton-Dissociation and Charge-Recombination Processes in Pentacene/C_{60} Solar Cells: Theoretical Insight into the Impact of Interface Geometry. *J. Am. Chem. Soc.* **2009**, *131*, 15777−15783.
(45) Clarke, T. M.; Durrant, J. R. Charge Photogeneration in Organic Solar Cells. *Chem. Rev. (Washington, DC, U.S.)* **2010**, *110*, 6736−6767.
(46) Hains, A. W.; Liang, Z.; Woodhouse, M. A.; Gregg, B. A. Molecular Semiconductors in Organic Photovoltaic Cells. *Chem. Rev. (Washington, DC, U.S.)* **2010**, *110*, 6689−6735.
(47) Gregg, B. A. Entropy of Charge Separation in Organic Photovoltaic Cells: The Benefit of Higher Dimensionality. *J. Phys. Chem. Lett.* **2011**, *2*, 3013−3015.
(48) Ahrens, M. J.; Sinks, L. E.; Rybtchinski, B.; Liu, W.; Jones, B.; Gaimo, J. M.; Gusev, A. V.; Goshe, A. J.; Tiede, D. M.; Wasielewski, M. R. Self-Assembly of Supramolecular Light-Harvesting Arrays from Covalent Multi-Chromophore Perylene-3,4:9,10-Bis(Dicarboximide) Building Blocks. *J. Am. Chem. Soc.* **2004**, *126*, 8284−8294.
(49) Li, C.; Wonneberger, H. Perylene Imides for Organic Photovoltaics: Yesterday, Today, and Tomorrow. *Adv. Mater.* **2012**, *24*, 613−636.
(50) Zhan, X.; Facchetti, A.; Barlow, S.; Marks, T. J.; Ratner, M. A.; Wasielewski, M. R.; Marder, S. R. Rylene and Related Diimides for Organic Electronics. *Adv. Mater.* **2011**, *23*, 268−284.
(51) Meng, L. Y.; Shang, Y.; Li, Q. K.; Li, Y. F.; Zhan, X. W.; Shuai, Z. G.; Kimber, R. G. E.; Walker, A. B. Dynamic Monte Carlo Simulation for Highly Efficient Polymer Blend Photovoltaics. *J. Phys. Chem. B* **2010**, *114*, 36−41.
(52) Mikroyannidis, J. A.; Stylianakis, M. M.; Sharma, G. D.; Bahraju, P.; Roy, M. S. A Novel Alternating Phenylenevinylene Copolymer with Perylene Bisimide Units: Synthesis, Photophysical, Electrochemical, and Photovoltaic Properties. *J. Phys. Chem. C* **2009**, *113*, 7904−7912.
(53) Rajaram, S.; Armstrong, P. B.; Kim, B. J.; Frechet, J. M. J. Effect of Addition of a Diblock Copolymer on Blend Morphology and Performance of Poly(3-Hexylthiophene):Perylene Diimide Solar Cells. *Chem. Mater.* **2009**, *21*, 1775−1777.
(54) Gao, B.-R.; Qu, J.-F.; Wang, Y.; Fu, Y.-Y.; Wang, L.; Chen, Q.-D.; Sun, H.-B.; Geng, Y.-H.; Wang, H.-Y.; Xie, Z.-Y. Femtosecond Spectroscopic Study of Photoinduced Charge Separation and Recombination in the Donor−Acceptor Co-Oligomers for Solar Cells. *J. Phys. Chem. C* **2013**, *117*, 4836−4843.
(55) Sharma, G. D.; Suresh, P.; Mikroyannidis, J. A.; Stylianakis, M. M. Efficient Bulk Heterojunction Devices Based on Phenylenevinylene Small Molecule and Perylene-Pyrene Bisimide. *J. Mater. Chem.* **2010**, *20*, 561−567.
(56) Mikroyannidis, J. A.; Stylianakis, M. M.; Suresh, P.; Sharma, G. D. Efficient Hybrid Bulk Heterojunction Solar Cells Based on Phenylenevinylene Copolymer, Perylene Bisimide and TiO_2. *Sol. Energy Mater. Sol. Cells* **2009**, *93*, 1792−1800.
(57) Sharma, G. D.; Balraju, P.; Mikroyannidis, J. A.; Stylianakis, M. M. Bulk Heterojunction Organic Photovoltaic Devices Based on Low Band Gap Small Molecule BTD-TNP and Perylene−Anthracene Diimide. *Sol. Energy Mater. Sol. Cells* **2009**, *93*, 2025−2028.
(58) Ramanan, C.; Smeigh, A. L.; Anthony, J. E.; Marks, T. J.; Wasielewski, M. R. Competition between Singlet Fission and Charge Separation in Solution-Processed Blend Films of 6,13-Bis-(triisopropylsilylethynyl)-pentacene with Sterically-Encumbered Perylene-3,4:9,10-bis(dicarboximide)s. *J. Am. Chem. Soc.* **2012**, *134*, 386−397.
(59) Howard, I. A.; Laquai, F.; Keivanidis, P. E.; Friend, R. H.; Greenham, N. C. Perylene Tetracarboxydiimide as an Electron Acceptor in Organic Solar Cells: A Study of Charge Generation and Recombination. *J. Phys. Chem. C* **2009**, *113*, 21225−21232.
(60) Keivanidis, P. E.; Howard, I. A.; Friend, R. H. Intermolecular Interactions of Perylene Diimides in Photovoltaic Blends of Fluorene Copolymers: Disorder Effects on Photophysical Properties, Film Morphology and Device Efficiency. *Adv. Funct. Mater.* **2008**, *18*, 3189−3202.
(61) Kim, I.; Haverinen, H. M.; Wang, Z. X.; Madakuni, S.; Li, J.; Jabbour, G. E. Effect of Molecular Packing on Interfacial Recombination of Organic Solar Cells Based on Palladium Phthalocyanine and Perylene Derivatives. *Appl. Phys. Lett.* **2009**, *95*, 023305-1−023305-3.
(62) Schlosser, F.; Sung, J.; Kim, P.; Kim, D.; Würthner, F. Excitation Energy Migration in Covalently Linked Perylene Bisimide Macrocycles. *Chem. Sci.* **2012**, *3*, 2778−2785.
(63) Lee, J.-L.; Stepanenko, V.; Yang, J.; Yoo, H.; Schlosser, F.; Bellinger, D.; Engels, B.; Scheblykin, I. G.; Würthner, F.; Kim, D. Structure−Property Relationship of Perylene Bisimide Macrocycles Probed by Atomic Force Microscopy and Single-Molecule Fluorescence Spectroscopy. *ACS Nano* **2013**, *7*, 5064−5067.
(64) Langhals, H.; Wagner, C.; Ismael, R. Star-Like Oriented Chromophores. *New J. Chem.* **2001**, *25*, 1047−1049.
(65) Pochas, C. M.; Kistler, K. A.; Yamagata, H.; Matsika, S.; Spano, F. C. Contrasting Photophysical Properties of Star-Shaped vs Linear Perylene Diimide Complexes. *J. Am. Chem. Soc.* **2013**, *135*, 3056−3066.
(66) Li, J.-B.; Yu, X.-L.; Fu, J.; Liu, X.; Zeng, Y. A Novel Perylene Diimide-Based Tetrahedral Molecule: Synthesis, Characterization and Self-Assembly with Gold Nanoparticles. *J. Chem. Sci.* **2010**, *122*, 839−846.
(67) Rao, K. V.; Haldar, R.; Kulkarni, C.; Maji, T. K.; George, S. J. Perylene Based Porous Polyimides: Tunable, High Surface Area with Tetrahedral and Pyramidal Monomers. *Chem. Mater.* **2012**, *24*, 969−971.
(68) Ganesan, P.; Baggerman, J.; Zhang, H.; Sudhoelter, E. J. R.; Zuilhof, H. Femtosecond Time-Resolved Photophysics of 1,4,5,8-Naphthalene Diimides. *J. Phys. Chem. A* **2007**, *111*, 6151−6156.
(69) Guide, M.; Pla, S.; Sharenko, A.; Zalar, P.; Fernández-Lázaro, F.; Sastre-Santos, Á.; Nguyen, T.-Q. A Structure−Property−Performance Investigation of Perylenediimides as Electron Accepting Materials in Organic Solar Cells. *Phys. Chem. Chem. Phys.* **2013**, *15*, 18894−18899.
(70) Yan, Q.; Zhou, Y.; Zheng, Y.-Q.; Pei, J.; Zhao, D. Towards Rational Design of Organic Electron Acceptors for Photovoltaics: A Study Based on Perylenediimide Derivatives. *Chem. Sci.* **2013**, *4*, 4389−4394.
(71) Shivanna, R.; Shoaee, S.; Dimitrov, S.; Kandappa, S. K.; Rajaram, S.; Durrant, J. R.; Narayan, K. S. Charge Generation and Transport in Efficient Organic Bulk Heterojunction Solar Cells with a Perylene Acceptor. *Energy Environ. Sci.* **2014**, *7*, 435−441.
(72) Jiang, W.; Ye, L.; Li, X.; Xiao, C.; Tan, F.; Zhao, W.; Hou, J.; Wang, Z. Bay-Linked Perylene Bisimides as Promising Non-Fullerene Acceptors for Organic Solar Cells. *Chem. Commun. (Cambridge, U.K.)* **2014**, *50*, 1024−1026.
(73) Wang, S.; Oldham, W. J.; Hudack, R. A.; Bazan, G. C. Synthesis, Morphology, and Optical Properties of Tetrahedral Oligo-(Phenylenevinylene) Materials. *J. Am. Chem. Soc.* **2000**, *122*, 5695−5709.
(74) Reichert, V. R.; Mathias, L. J. Expanded Tetrahedral Molecules from 1,3,5,7-Tetraphenyladamantane. *Macromolecules* **1994**, *27*, 7015−7023.
(75) Bullock, J. E.; Vagnini, M. T.; Ramanan, C.; Co, D. T.; Wilson, T. M.; Dicke, J. W.; Marks, T. J.; Wasielewski, M. R. Photophysics and Redox Properties of Rylene Imide and Diimide Dyes Alkylated Ortho to the Imide Groups. *J. Phys. Chem. B* **2010**, *114*, 1794−1802.

(76) Kim, C. H.; Joo, T. Ultrafast Time-Resolved Fluorescence by Two Photon Absorption Excitation. *Opt. Express* **2008**, *16*, 20742−20747.
(77) Rhee, H.; Joo, T. Noncollinear Phase Matching in Fluorescence Upconversion. *Opt. Lett.* **2005**, *30*, 96−98.
(78) Lefler, K. M.; Brown, K. E.; Salamant, W. A.; Dyar, S. M.; Knowles, K. E.; Wasielewski, M. R. Triplet State Formation in Photoexcited Slip-Stacked Perylene-3,4:9,10-bis(dicarboximide) Dimers on a Xanthene Scaffold. *J. Phys. Chem. A* **2013**, *117*, 10333−10345.
(79) Ford, W. E.; Kamat, P. V. Photochemistry of 3,4,9,10-Perylenetetracarboxylic Dianhydride Dyes. 3. Singlet and Triplet Excited-State Properties of the Bis(2,5-di-*tert*-butylphenyl)imide Derivative. *J. Phys. Chem.* **1987**, *91*, 6373−6380.
(80) Veldman, D.; Chopin, S. M. A.; Meskers, S. C. J.; Groeneveld, M. M.; Williams, R. M.; Janssen, R. A. J. Triplet Formation Involving a Polar Transition State in a Well-Defined Intramolecular Perylenediimide Dimeric Aggregate. *J. Phys. Chem. A* **2008**, *112*, 5846−5857.
(81) Seibt, J.; Marquetand, P.; Engel, V.; Chen, Z.; Dehm, V.; Würthner, F. On the Geometry Dependence of Molecular Dimer Spectra with an Application to Aggregates of Perylene Bisimide. *Chem. Phys.* **2006**, *328*, 354−362.
(82) Kasha, M.; Rawls, H. R.; El-Bayoumi, M. A. The Exciton Model in Molecular Spectroscopy. *Pure Appl. Chem.* **1965**, *11*, 371−392.
(83) Wu, Y.-L.; Brown, K. E.; Wasielewski, M. R. Extending Photoinduced Charge Separation Lifetimes by Using Supramolecular Design: Guanine−Perylenediimide G-Quadruplex. *J. Am. Chem. Soc.* **2013**, *135*, 13322−13325.
(84) Gunderson, V. L.; Mickley Conron, S. M.; Wasielewski, M. R. Self-Assembly of a Hexagonal Supramolecular Light-Harvesting Array from Chlorophyll a Trefoil Building Blocks. *Chem. Commun. (Cambridge, U.K.)* **2010**, *46*, 401−403.
(85) Kelley, R. F.; Goldsmith, R. H.; Wasielewski, M. R. Ultrafast Energy Transfer within Cyclic Self-Assembled Chlorophyll Tetramers. *J. Am. Chem. Soc.* **2007**, *129*, 6384−6385.
(86) Varnavski, O. P.; Ostrowski, J. C.; Sukhomlinova, L.; Twieg, R. J.; Bazan, G. C.; Goodson, T. Coherent Effects in Energy Transport in Model Dendritic Structures Investigated by Ultrafast Fluorescence Anisotropy Spectroscopy. *J. Am. Chem. Soc.* **2002**, *124*, 1736−1743.
(87) Valeur, B. *Molecular Fluorescence*; Wiley-VCH: Weinheim, Germany, 2002.
(88) Tao, T. Time-Dependent Fluorescence Depolarization and Brownian Rotational Diffusion Coefficients of Macromolecules. *Biopolymers* **1969**, *8*, 609−632.
(89) Lakowicz, J. R. *Principles of Fluorescence Spectroscopy*; Kluwer: Dordrecht, The Netherlands, 1999.
(90) Turro, N. J. *Modern Molecular Photochemistry*; University Science Books: Sausalito, CA, 1991.